ACS APPLIED MATERIALS & INTERFACES

www.acsami.org

Research Article

Fabrication of Multilayered Composite Nanofibers Using Continuous Chaotic Printing and Electrospinning: Chaotic Electrospinning

Sunshine Holmberg,* Norma Alicia Garza-Flores, Mohammad Ali Almajhadi, Carolina Chávez-Madero, Alejandro Lujambio-Angeles, Binny Jind, Claudia Bautista-Flores, Christian Mendoza-Buenrostro, Esther Pérez-Carrillo, Hemantha Kumar Wickramasinghe, Sergio Omar Martínez-Chapa,* Marc Madou, Paul S. Weiss, Mario Moisés Álvarez, and Grissel Trujillo-de Santiago*

Cite This: *ACS Appl. Mater. Interfaces* 2021, 13, 37455−37465

Read Online

ACCESS | Metrics & More | Article Recommendations | Supporting Information

ABSTRACT: Multi-material and multilayered micro- and nanostructures are prominently featured in nature and engineering and are recognized by their remarkable properties. Unfortunately, the fabrication of micro- and nanostructured materials through conventional processes is challenging and costly. Herein, we introduce a high-throughput, continuous, and versatile strategy for the fabrication of polymer fibers with complex multilayered nanostructures. Chaotic electrospinning (ChE) is based on the coupling of continuous chaotic printing (CCP) and electrospinning, which produces fibers with an internal multi-material microstructure. When a CCP printhead is used as an electrospinning nozzle, the diameter of the fibers is further scaled down by 3 orders of magnitude while preserving their internal structure. ChE enables the use of various polymer inks for the creation of nanofibers with a customizable number of internal nanolayers. Our results showcase the versatility and tunability of ChE to fabricate multilayered structures at the nanoscale at high throughput. We apply ChE to the synthesis of unique carbon textile electrodes composed of nanofibers with striations carved into their surface at regular intervals. These striated carbon electrodes with high surface areas exhibit 3- to 4-fold increases in specific capacitance compared to regular carbon nanofibers; ChE holds great promise for the cost-effective fabrication of electrodes for supercapacitors and other applications.

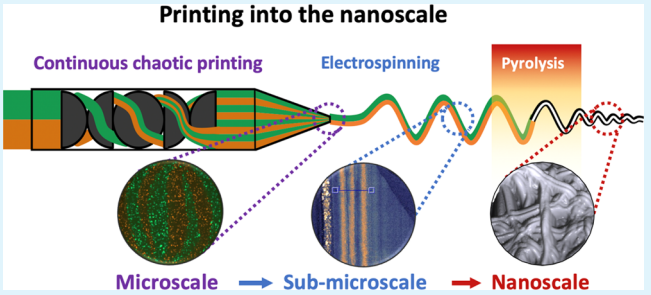

KEYWORDS: *chaotic printing, electrospinning, nanofabrication, multi-material, multilayered, supercapacitors, carbon nanostructures*

Layered micro- and nanostructures figure prominently in nature. While varying in color, shape, size, and composition, they share extensive interfaces in one, two, or three dimensions.[1−4] These multi-scale and multi-material structures may provide remarkable properties and functionalities (*i.e.*, support, structure, orientation, mass transfer, and interfacial connection) that are crucial for many purposes.[1−3,5,6] These architectures have inspired countless research contributions dedicated to mimicking their structures and compositions to harness their highly efficient and exceptional electrical, chemical, physical, optical, and structural properties.[7−9] In the field of micro-electro-mechanical systems and nanotechnology, there is growing interest in fabricating such multifunctional constructs for applications in optical imaging,[10−12] catalysis,[13−15] drug delivery,[16−18] sensing,[12,19,20] micro-motors,[18,19,21] and water purification.[21]

Among the various nanofabrication technologies, electrohydrodynamic (EHD) jetting techniques (and electrospinning in particular) stand out due to their versatility and scalability.[5,22,23] By altering the modality of the techniques, the jetting process can rapidly produce nanoparticulate coatings or nanofibrous mats in simple and scalable fabrication systems. With appropriate post-treatment processes, the material composition of the formed nanostructures can be adjusted, enabling the syntheses of materials ranging from polymers to metals, ceramics, and carbons.[22−25] In addition to its versatility in creating nanostructures of varying morphology and material composition, EHD jetting can be used to fabricate multilayered or multiphase nanostructures by exploiting the physical and chemical behaviors of its precursor solutions. However, current multilayer EHD jetting processes are mainly limited to techniques exploiting phase separation, such as water−oil emulsions, or chemical separation (such as that seen in block-copolymers).[26−30]

Received: March 23, 2021
Accepted: July 14, 2021
Published: August 2, 2021

https://doi.org/10.1021/acsami.1c05429
ACS Appl. Mater. Interfaces 2021, 13, 37455−37465

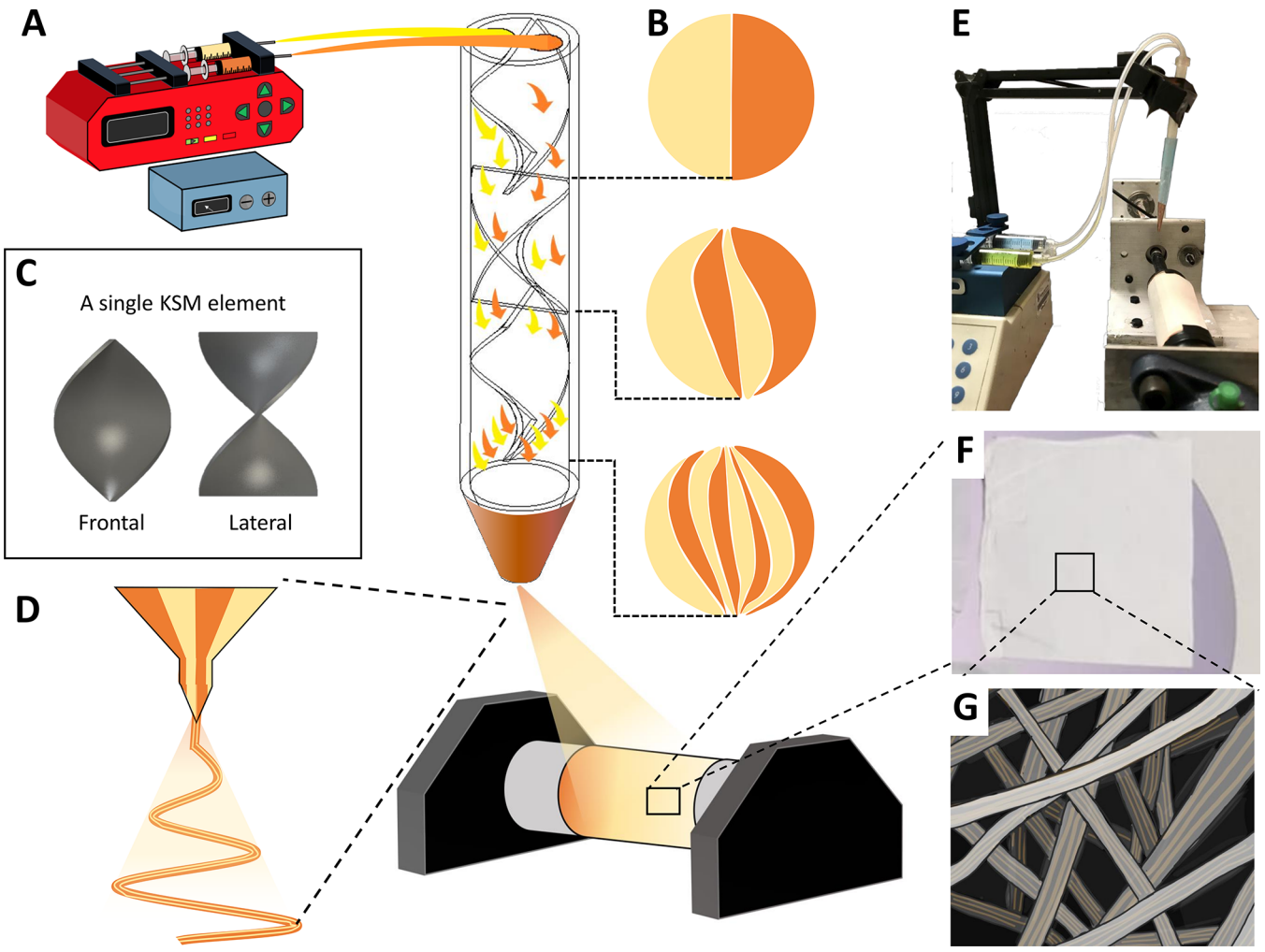

Figure 1. ChE setup. (A) Schematic of the ChE setup: a syringe pump feeds two polymer solutions at constant rates into a CCP system using an injection pump. (B) CCP system, which contains three KSM elements, originates the microstructure within the polymer-extruded fiber by chaotic advection. (C) Helicoidal design of a single KSM mixing element (frontal and lateral views are shown). The fiber is then electrospun as a nanofiber mat. Intercalated layered architecture formed by the two-polymer stream at different cross sections along the KSM. (D) Schematic of the Taylor cone formation at the spinneret and the preservation of the layered nanostructure within the jet. (E) Actual ChE system setup. (F) Photograph of the resultant nanofiber mat. (G) Schematic of the fibrous mat composed of nanofibers with an internal nanostructure.

Herein, we describe and demonstrate a versatile EHD jetting-based methodology for fabricating multilayered nanostructures in a simple, rapid, and continuous process. Chaotic electrospinning (ChE) is an innovative fabrication technique that combines electrospinning with continuous chaotic printing (CCP). CCP is a recently developed technology that uses chaotic static mixers as printing nozzles to produce micron-sized filaments with internal multilayered structures by extrusion. This technology is based on the deterministic chaotic advection of flows that allows the exponential creation of a microlayered structure inside a static mixer in a controlled and predictable manner.[5,22] Electrospinning, meanwhile, spans from the micro- to the nanoscale. This transition from the micro- (CCP) to the nanoscale (electrospinning) challenges the preservation of the multilayered structure achieved by CCP within the extruded filament due to the drastic changes in velocity when the jet is formed. In this regard, we studied the roles of the rheological properties of the polymer combinations used in the preservation of the internal multilayered structure and found suitable conditions for fabricating electrospun fibers with multilayered nanostructures. We demonstrated the use of ChE to create carbon nanofibers (CNFs) with multilayered parallel carved patterns. These CNFs were fabricated by utilizing two polymers, one that could be carbonized through pyrolysis and a sacrificial one that is completely removed during pyrolysis. The resulting carbon is a textile composed of striated CNFs (SCNFs), with greatly enhanced surface area. The augmentation in the surface area provided by the internal structures of these CNFs boosted their performance as electrodes for energy-storage applications, such as in supercapacitors. In this regard, the results presented here suggest that ChE is an effective step toward circumventing current limitations for synthesizing multiscale nanostructures and provides the necessary versatility, flexibility, and high yield that are needed in many engineering applications.

RESULTS AND DISCUSSION

ChE combines CCP technology[31] and far-field electrospinning into a versatile and scalable nanofabrication technique for synthesizing nanofibers with internal multilayered structures. Initially, alternating microlayers of two flowing materials are formed inside a chaotic static mixer and are then extruded

https://doi.org/10.1021/acsami.1c05429
ACS Appl. Mater. Interfaces 2021, 13, 37455−37465

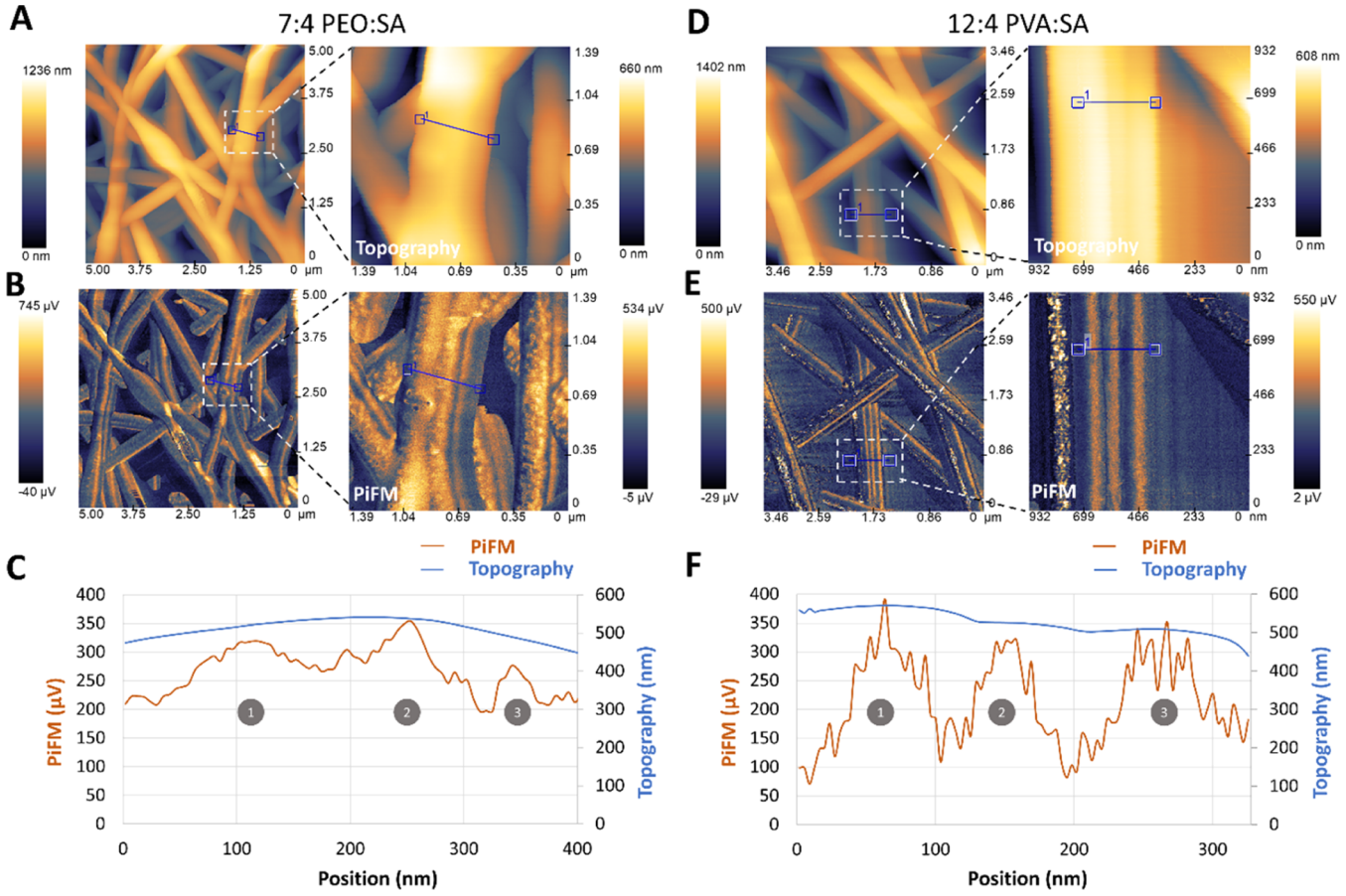

Figure 2. AFM and PiFM characterization of ChE-produced nanofibers using a three-element-KSM printhead. (A) 7% PEO/4% SA nanofibers analyzed by AFM and (B) PiFM and (C) intensity profiles of lines indicated in the micrographs. (D) 12% PVA/4% SA nanofibers analyzed by AFM and (E) PiFM and (F) intensity profiles exhibited by the fibers along the lines indicated in the micrographs.

through the spinneret, where the electrospinning jetting stretches the chaotic structure down to the nanoscale (Figure 1).

Although EHD co-jetting processes for the synthesis of multiphase structures have been widely explored, these techniques often employ chemical- or phase-based separation methods such as oil-water emulsions or block-copolymers.[32−34] Alternatively, ChE achieves defined layered architectures by splitting and folding fluid streams in the laminar regime (chaotic advection). The polymer solutions remain segregated because the laminar regime is preserved both during the CCP and the electrospinning process. Thus, our fluid-based fabrication method opens a new window of unprecedented possibilities not achievable by current chemical- or phase-separation processes.

Chaotic Electrospinning Setup. We illustrate the concept and setup of our ChE system in Figure 1A. The process comprises two main stages: CCP and electrospinning. The CCP occurs within a static mixer where the chaotic advection of two different flowing polymers creates intercalated layered structures (Figure 1B). The static mixer used here, a Kenics static mixer (KSM), contains a sequential set of helicoidal mixing elements (Figure 1C) placed at 90° with respect to one another that split and reorient the flowing materials, creating layers in an exponential fashion along the tube (Figure 1B). This KSM was custom 3D-printed as a single-piece unit containing a cap with two inlets, a cylindrical pipe that ends in a conical dispensing tip, and three KSM-elements inside the pipe. This setup (Figure 1E) produces filaments with eight internal and intercalated layers of the two fed flowing materials.

The process of generation of the microstructure during chaotic printing has been detailed in recent reports.[31,35−37] Briefly, each KSM element (Figure 1C) within the printhead sequentially reorients and splits the incoming flow into two streams (Figure 1B). The two streams of distinct materials originally fed at the top of the printhead are only reoriented in the first element and reoriented and divided into four intercalated layers by the action of the second KSM element. These four layers will split into eight intercalated layers by the action of the third KSM element. This sequential splitting can be iteratively repeated to duplicate the number of layers by adding KSM elements to the printhead.

For the second stage, electrospinning, copper tape was wrapped around the tip of the conical dispenser. The entire CCP-spinneret system is held 10 cm above a rotating drum spinning at 5 revolutions per second (rps) that acts as the nanofiber collector. In operation, the two polymer solutions are dispensed through silicone tubing into the KSM downstream at a constant rate (0.2 mL/h) controlled by a syringe pump. A high-voltage power source drives the electric field between the drum and the spinneret. The electric field stretches the polymer meniscus at the tip of the spinneret, forming the Taylor cone. The electrospinning jet emits from the Taylor cone (Figure 1D), jetting the polymer solution into a continuous nanofiber as it travels to the collector and forms a

https://doi.org/10.1021/acsami.1c05429
ACS Appl. Mater. Interfaces 2021, 13, 37455−37465

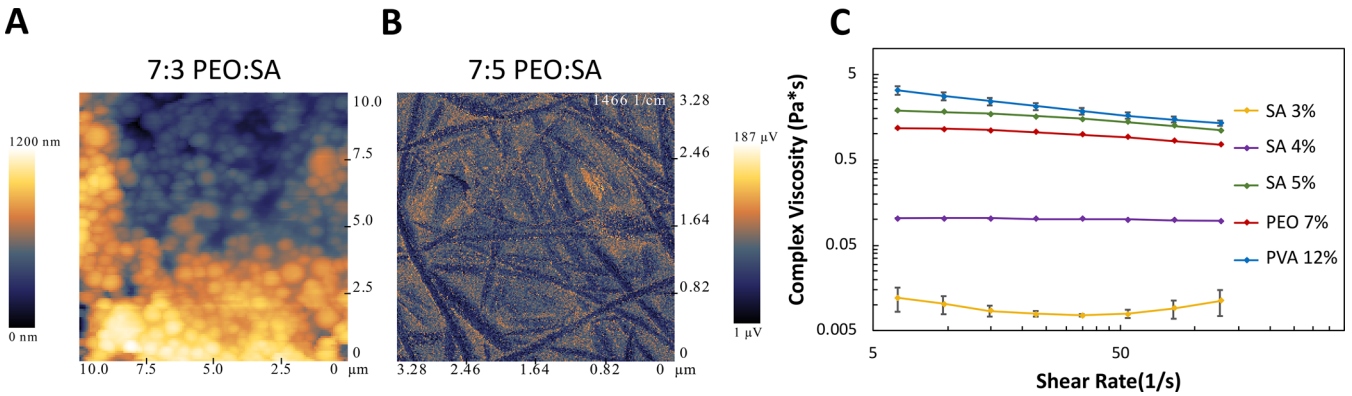

Figure 3. PiFM and rheological characterization of other solutions tested for ChE compatibility. (A) AFM and PiFM analysis of 7% PEO/3% SA and (B) 7% PEO/5% SA nanofibers. (C) Rheology analysis of the polymer solution tested in the ChE system.

nanofibrous textile (Figure 1F) with an inner-microlayered structure (Figure 1G).

We conducted an extensive and systematic set of preliminary ChE experiments, using different combinations of polymers (Supporting Information, Table 1) and identified several key requirements that must be satisfied to ensure the successful fabrication of multilayered nanostructured fibers. In this regard, an optimal polymer combination must enable the laminar coextrusion in the CCP system (*i.e.*, polymers must exhibit interfacial and rheological compatibility), be electrospinnable (*i.e.*, at least one polymer must be sufficiently conductive), and offer a proper balance between elastic and viscous forces for the system to create coherent nanofibers with an internal microlayered structure.

Nanolayered Fiber-Fabrication and Photoinduced Force Microscopy Characterization. Next, we demonstrate the fabrication of polymer fibers that exhibit internal layered structures at the nanoscale using two combinations of aqueous-polymer solutions, (a) 7% poly(ethylene oxide) and 4% sodium alginate (PEO/SA) and (b) 12% poly(vinyl alcohol) and 4% sodium alginate (PVA/SA) (Figure 2; Supporting Information, Figure 1). For the PVA/SA blend, sodium dodecyl sulfate (SDS) was added to the PVA solution to increase the conductivity of the PVA/SA polymer and facilitate electrospinning. From all polymer combinations that we analyzed (Supporting Information, Table 1), these exhibited the best working properties to produce flawless (*i.e.*, bead-less and continuous) electrospun nanofibers by ChE. The electric field was determined by the lowest working voltage that would enable stable and continuous EHD jetting. For the PEO/SA combination, the working voltage was 10 kV, while 12 kV was used for the PVA/SA combination.

Atomic force microscopy (AFM) was used to characterize the topography of our electrospun textiles, while photoinduced force microscopy (PiFM) was employed as the primary characterization tool to visualize the alternating layers of different compositions within them. PiFM is a noninvasive, highly sensitive, and versatile technique that enables nanoscale chemical imaging with *ca.* 10 nm spatial resolution.[38,39] A mechanical cantilever's probe tip samples and is used to map the surface through local light−matter interactions. The excitation wavelength is tuned to correspond to vibrational resonances of the material under study. The technique has proven useful for the analysis of heterogeneous samples such as block-copolymers with signal-to-noise ratios.[40] For this work, PiFM was used to identify internal layers formed within each nanofiber by differentiating between the PEO or PVA and SA layers through differences in their spectral signatures.

The micrographs obtained from the AFM and PiFM analyses of the nanofibrous textiles are shown in Figure 2. Figure 2A,D shows the topographic maps of each nanofiber, as determined by the AFM. Figure 2B,E shows the juxtaposition of the AFM topography and the composition map measured by the PiFM. SA layers are shown in gold (~500−750 μV) and PEO or PVA (~0 μV) in blue. We were able to differentiate the multiple layers of the PEO/SA and PVA/SA fibers. These results demonstrate the feasibility of extending the CCP technique to the nanoscale. Figure 2C,F and Supporting Information, Figure 1 show the intensity profiles along the lines indicated in the AFM and PiFM micrographs. This analysis indicates that ChE was able to produce flawless fibers and preserve the multilayered internal structure developed during the CCP stage. However, not all combinations of polymer blends tested were successful (Figure 3). Combinations such as 7% PEO/3% SA were incapable of forming nanofibers (Figure 3A), while others, such as 7% PEO/5% SA, successfully formed nanofibers, but no internal structure was observed (Figure 3B).

Next, we discuss how the properties of the polymer solutions used in ChE determine the success of this manufacturing method.

Influence of Polymer Properties on Generating Structured Nanofibers. Several criteria need to be met in order to produce multilayer-structured nanofibers using ChE. Both stages of the process, CCP and electrospinning, require the use of polymer blends with specific properties to be successfully processed into nanofibers with internal layered architectures. For CCP, the combination of polymer solutions should be compatible in terms of interfacial tension and polarity.[31] Additionally, both flowing materials should behave as Newtonian liquids within the window of shear rates that they experience when extruded along the mixer. This compatibility and Newtonian behavior enable the polymer solutions to flow stably side-to-side (without mixing), creating defined layers during CCP.[31] For the electrospinning stage, the blend must exhibit adequate ionic conductivity and viscoelastic profile to establish and to sustain the electrospinning jet and produce coherent nanofibers steadily.[5,22]

Moreover, ChE involves additional challenges. The polymer blend is subject to a substantial change of velocity (therefore, shear-stress values) when transitioning from the micro (CCP) to the nano (electrospinning) domain. The electrospinning

https://doi.org/10.1021/acsami.1c05429
ACS Appl. Mater. Interfaces 2021, 13, 37455−37465

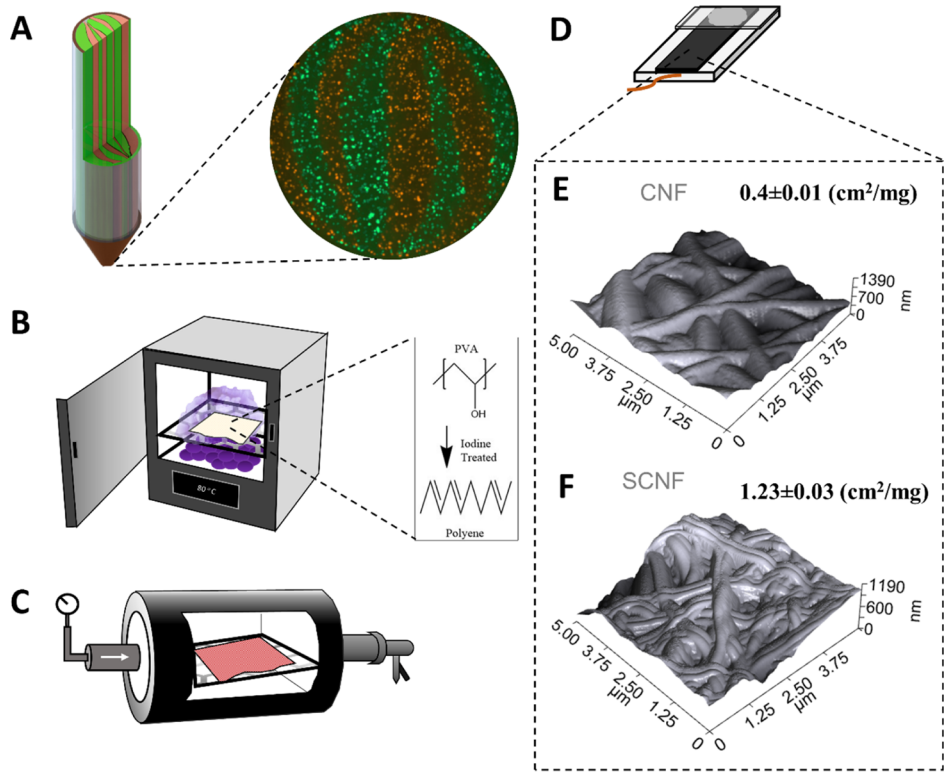

Figure 4. Fabrication of SCNFs and AFM characterization of their morphology. (A) CCP of microstructured and multilayered microfibers of polymer blends that contain alternating layers of red and green microparticles (for visualization purposes). These fibers are then continuously electrospun. Chaotically electrospun fibers, containing layers of 12% poly(vinyl alcohol) (PVA)/4% SA, were stabilized and carbonized. (B) Crosslinking of PVA *via* incubation in iodine vapor at 80 °C. (C) Carbonization of the PVA/SA nanofibers in a tube furnace under constant nitrogen flow. (D) Resulting SCNFs are wired by attaching a copper wire *via* silver paste and then covering the contact area with polydimethylsiloxane (PDMS). AFM topological characterization of the (E) CNF electrodes and the (F) SCNF electrodes.

solution is extremely confined at the Taylor cone, where the polymer meniscus at the tip of the spinneret transitions into the electrospinning jet.[32,41,42] This transition enables a 3 orders of magnitude change in the surface-to-volume ratio of the polymer solution over less than a few microns. In order to preserve the internal layered structure even when the blend is rapidly pulled from the Taylor cone, the polymers should keep flowing as Newtonian liquids within the laminar regime. Considering these requirements, we used water-polymer solutions to comply with the interfacial and polar compatibility that CCP demands. For electrospinning, we used polymer pairs previously reported as electrospinnable elsewhere.[43,44] Here, PVA and PEO were used as carriers to confer electrospinnability to the blend, since SA itself is not electrospinnable.[6,44−46] We observed that, among all tested polymer blends, only the blends containing 4% SA were successful in producing coherent electrospun nanofibers with internal layered structures, as confirmed by the PiFM analysis. Aiming to understand the mechanism behind this finding, we individually characterized the complex viscosity of all our polymer blends using a rotational, cone-plate rheometer at a wide range of shear rate values (6.28−126 1/s) (Figure 3C). Among all polymer solutions, 4% SA was the only one showing a steady Newtonian behavior (invariable viscosity) in the range of shear-stress values tested (Figure 3C). These results suggest that 4% SA acts as a "stabilizer" for the flow and allows the blend to keep flowing in the laminar regime throughout the ChE process. Even when PVA or PEO behaves as a non-Newtonian material at different shear rates, our results suggest that the presence of 4% SA provides sufficient stability to the polymer blend to preserve the laminar regime. Rheological characterization also suggests that the SA concentration has an important effect on both the electrospinnability and preservation of the internal microlayered structure. When using 3% SA solutions, the polymer blend did not exhibit sufficient strength (viscosity) to produce coherent nanofibers; instead, the material was sprayed from the KSM to the rotating drum creating a mat formed of beads (Figure 3A). When using 5% SA solutions, nanofibers were successfully obtained, but no internal layered structure was evident in our PiFM analysis (Figure 3B). The viscosity profile of 5% SA solution exhibited non-Newtonian behavior in the range of shear-stress values tested (Figure 3C). The increased concentration of SA (as compared to 4% SA) may have added elastic forces that counteract when pulled from the Taylor cone, generating micro-eddies and destroying the structure formed within the KSM.

The 5% SA solutions, in combination with the PEO or PVA solutions, may have rendered a viscoelastic blend incapable of sustaining the flow laminarity in the CCP-electrospinning transition; therefore, non-structured (well-mixed) nanofibers were obtained. A closer examination of Figure 2B,E shows that the PVA/SA polymer combination exhibited more defined layers. The higher viscosity of 12% PVA as compared to that of 7% PEO solutions (Figure 3C) may have contributed to the formation of more coherent nanofibers and reduction in mixing with 4% SA, preserving the internal structure. The

https://doi.org/10.1021/acsami.1c05429
ACS Appl. Mater. Interfaces 2021, 13, 37455−37465

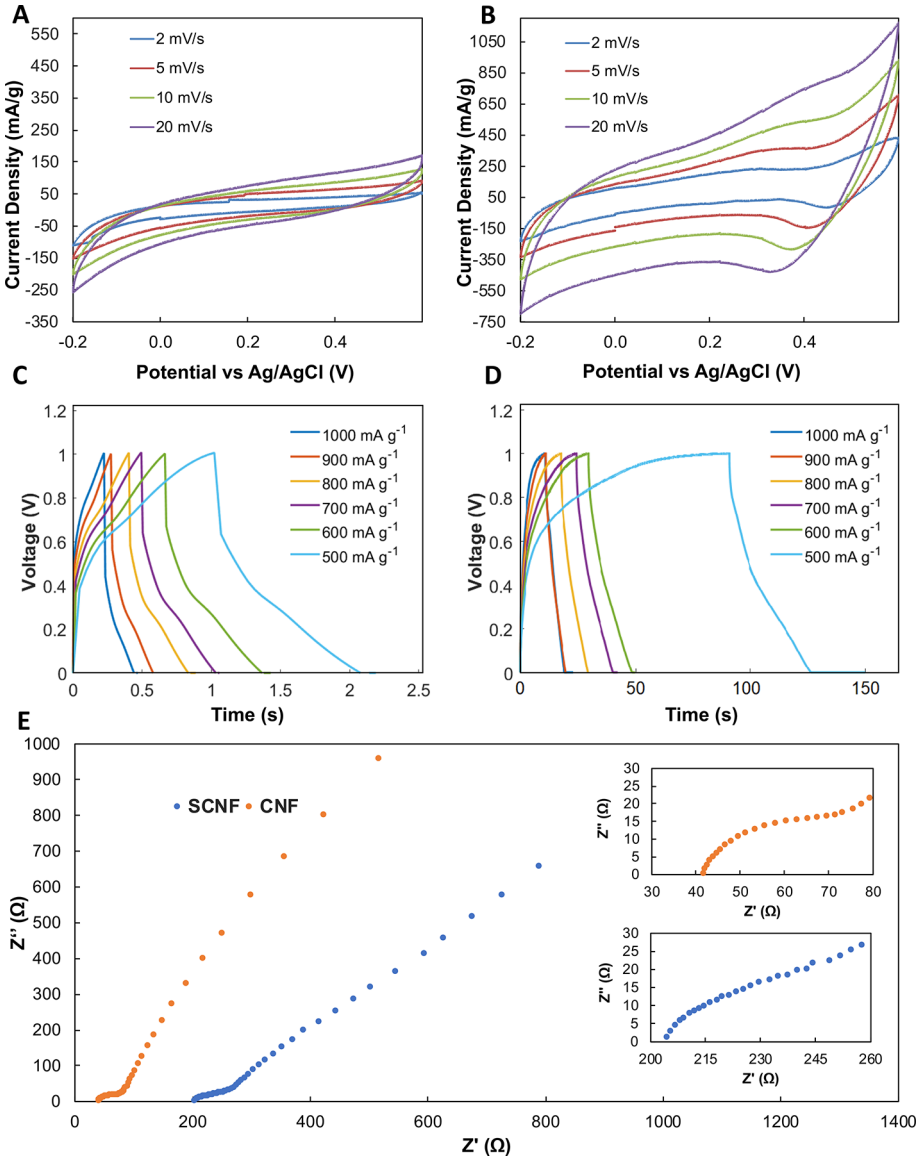

Figure 5. Voltametric and galvanostatic characterization of the supercapacitive behavior of SCNFs. Representative cyclic voltammograms of (A) CNF (red) and (B) SCNF (blue) in 2 M MgCl aqueous solutions at scan rates of 2, 5, 10, and 20 mV/s. Representative GCD curves of (C) CNF and (D) SCNF as measured in 2 M MgCl aqueous solutions at constant currents of 500, 600, 700, 800, 900, and 1000 mA g^{-1}. (E) Representative EIS of CNF orange) and SCNF (blue) electrodes in aqueous 2 M MgCl. Insets zoom in the high-frequency regions.

rheological characterization for all polymer solutions tested is presented in the Supporting Information, Figure 2.

Based on these observations, a basic framework can be laid out for ChE. For two-polymer-based ChE systems, the preservation of the chaotic internal structures requires a polymer blend that is: (1) compatible in terms of interfacial tension and polarity, (2) electrospinnable into coherent nanofibers, and (3) Newtonian within a wide range of shear rates of the whole ChE process.

According to the aforementioned criteria, ChE has the potential to be one of the most versatile nanofabrication methods for producing such multilayered structures.

Supercapacitor Fabrication and Characterization. To demonstrate the applicability of the ChE technique, we exploited the carbonizable properties of PVA to produce CNFs *via* pyrolysis, which allows the formation of internal layered cavities by the decomposition of the SA layers of the nanofiber. These as-fabricated SCNFs, with their etched cavities, feature a higher surface area than in typical CNFs, thus making them useful for energy-storage applications. The SCNFs are electrochemically characterized and compared to CNFs to explore their use for applications such as supercapacitor electrodes.

The primary function of supercapacitors as energy-storage devices is to provide high power density for rapid charging and discharging in electrical and electronic devices. This function is achieved through the way supercapacitors store their charges in the electric double layer. The electric double layer is a nanometer-thick sheet of ionic charge that forms along the interface between the electrode and electrolyte in a supercapacitor cell. Due to the short distance of travel, the electric double layer can provide rapid dissipation and accumulation of charges. Therefore, the most direct way to increase the performance of supercapacitors is to increase this interfacial surface area, while simultaneously reducing superfluous volumetric density. In this regard, the extra surface area

https://doi.org/10.1021/acsami.1c05429
ACS Appl. Mater. Interfaces 2021, 13, 37455−37465

created through the pyrolysis of the chaotic PVA/SA nanofibers should provide significant improvement in supercapacitance over conventionally electrospun CNFs.

The SCNFs were produced from the ChE 12% PVA/4% SA polymer nanofibers with a KSM printhead with three mixing elements (Figure 4A). The PVA/SA and pure PVA nanofiber mats were incubated in an iodine-rich environment at 80 °C for 24 h to stabilize PVA's carbon backbone into polyene (Figure 4B). This step has been demonstrated in prior studies to be necessary for providing enough carbon−carbon bonds and to prevent the disintegration of PVA during pyrolysis.[47] Finally, the fibers are carbonized in a tube furnace under continuous ultrapure, nitrogen-rich flow at 1000 °C (Figure 4C). Electrical contacts are made with the carbon electrodes by attaching a copper wire to its surface *via* a conductive silver ink, and the entire contact area is then encased in silicone rubber to prevent corrosion (Figure 4D). Comparison of the morphology between CNFs and SCNFs (Figure 4E,F) using AFM shows cavities in the centers of the fiber structures in the SCNFs, which are not present in the CNF samples. We further used the AFM topological profiles along the lines to calculate the surface area (A) per unit of mass (m) of each type of fiber textile (CNFs and SCNFs) (Supporting Information, Figure 3). To that aim, we computed a surface integral (eq 1) that resembles the arc-length integral for 2D surfaces.

$$\frac{A}{m} = \frac{1}{m}\int_0^w \sqrt{1 + \left(\frac{\delta}{\delta x} f(x, y)\right)^2 + \left(\frac{\delta}{\delta y} f(x, y)\right)^2}\, dx\, dy \tag{1}$$

In eq 1, $f(x,y)$ is the height at positions x and y from the AFM profiling data along a given line across the surface and w is the width of the surface. The results demonstrate a 3-fold increase in the specific surface area of the SCNF samples over the CNF samples (Figure 4E,F; Supporting Information, Figure 3), which should translate to a comparable increase in the capacitance of their respective electrodes.

Half-cell supercapacitor characterization was conducted using a three-electrode electrochemical setup. Figure 5 shows the results of the electrochemical characterization of the SCNF and CNF electrodes. The gravimetric specific capacitance can be extracted from cyclic voltammetry (CV) (Figure 5A,B) with eq 2

$$C_p = Am^{-1}v^{-1}\Delta V^{-1} \tag{2}$$

here, C_p is the specific capacitance, A is the integrated area under the CV curve, m is the mass of the carbon electrodes, v is the scan rate, and ΔV is the potential window of the CV sweep. To evaluate the rate performance of the SCNF and CNF electrodes, galvanostatic charge−discharge (GCD) was conducted at current densities of 500, 600, 700, 800, 900, and 1000 mA g^{-1}. From the collected data (Figure 5C,D), the gravimetric specific capacitance can be calculated from eq 3

$$C_g = Itm^{-1}\Delta V^{-1} \tag{3}$$

here, I ([=] A) is the discharge current, t ([=] s) is the discharge time, m ([=] g) is the mass of the carbon fiber electrodes, and ΔV ([=] V) is the potential change during the discharge process. Interestingly, the small peaks visible in the cyclic voltammograms of both SCNF and, to a lesser extent, CNF electrodes reveal the presence of faradaic reactions from pseudocapacitance. The presence of pseudocapacitance is also seen in the lack of symmetry between the charging and discharging in the GCD curves. Pseudocapacitance can be present in pyrolytic carbons due to retained functional groups from the carbon precursor,[48,49] such as the alcohol groups in PVA. The additional faradaic reactions enhance the measured capacitance beyond that normally seen in purely electrostatic interactions, as in the case of the double-layer capacitance. Electrochemical impedance spectroscopy (EIS) was used to decouple the enhancement in capacitance between the pseudocapacitance and that of the electric double layer (Figure 5E). By fitting the EIS plots to an equivalent circuit (Supporting Information, Figure 4) model, the value of the double-layer capacitance can be extrapolated.[50]

From the analysis of the CV curves shown in Table 1, it is seen that the SCNF electrodes exhibit more than a 4-fold increase over the measured capacitance of the CNF. Once the pseudocapacitance is factored out, a greater difference in capacitance is observed between SCNFs and CNFs, where SCNFs exhibited over 3-fold greater electrostatic capacitance than CNFs, reflecting the enhancement in the surface area created by the combination of ChE and pyrolysis. In comparison with other electrospun CNF studies, SCNFs exhibit similar specific capacitance despite no additional activation or functionalization steps after pyrolysis.[23,51,52] From the analysis of the GCD, we observed that SCNFs have a remarkably higher capacitance retention (*i.e.*, 16% at 1000 mA g^{-1}) than CNFs (*i.e.*, 1.8% retention at 1000 mA g^{-1}). This suggests that the architectural change that ChE and pyrolysis induced at the nanoscale improved the diffusion of electrolyte ions.[53] These results demonstrate the potential of this nanofabrication technology, with capabilities for greater enhancements in capacitance with additional metal oxides, activation and functionalization steps, and KSM elements during the ChE process.

Table 1. Capacitance of CNFs and SCNFs

	capacitance (F/g) (CV) @ (2 mV/s)	capacitance (F/g) (GCD) @ (1 A g^{-1})	capacitance (F/g) (EIS)
CNF	13.3 ± 3.2	0.225 ± 0.0006	7.1 ± 3.92
SCNF	55.3 ± 31.2	8.477 ± 0.331	19.5 ± 10.7

CONCLUSIONS AND PROSPECTS

In this work, we describe and demonstrate a versatile and scalable nanofabrication process that combines CCP technology and electrospinning to produce multilayered nanofibers. These nanostructures are created by feeding two polymer streams into a customized KSM, where chaotic advection creates intercalated layered structures at an exponential rate. A large electric field is then applied between the extruding tip of the KSM and the collector, a rotating drum. The electric field induces the formation of nanofibers from the chaotic extruder outlet, which are then deposited continuously on the collector and form a textile-like mat. Scanning electron microscopy (SEM) and PiFM techniques were used to demonstrate ChE proficiency in manufacturing multilayered nanofibers in a facile and economical manner.

In this study, we used PVA, PEO, and SA, which are all polymers soluble in water with interfacial compatibilities that allow extrusion and structure generation by CCP. SA solutions are not themselves electrospinnable, but the addition of PVA (enriched with SDS) or PEO as carrier facilitates the

https://doi.org/10.1021/acsami.1c05429
ACS Appl. Mater. Interfaces 2021, 13, 37455−37465

electrojetting process. Among the blends of polymers tested, 7% PEO/4% SA and 12% PVA/4% SA led to the targeted layered architectures inside the nanofibers. We attribute this result mainly to the Newtonian behavior of 4% SA observed in a wide range of shear-stress values, as evaluated by rheological analyses. Consistently, this was the only polymer solution tested that exhibited Newtonian behavior throughout the entire range of shear-stress evaluated.

The 4% SA solutions acted as stabilizers of the flow, preserving the laminar regime of the blend throughout the entire ChE process, even when transitioning from the microscale domains (CCP outlet) to nanoscale domains (electrospinning) at the Taylor cone. Furthermore, our results suggest that viscosity should be appropriately tuned in order to facilitate coherent nanofibers through the electrospinning process and to preserve the laminar flow and therefore the internal microarchitecture. Further analyses are necessary to understand the phenomena underlying ChE and their interplay.

To demonstrate a potential application of ChE, the PVA/SA chaotic nanofibers were pyrolyzed to create carbon fibers with striated cavities etched onto their surfaces. These SCNFs exhibited large surface areas, which made them potential candidates for energy-storage devices, such as supercapacitors. The SCNF electrodes were then electrochemically characterized for their specific capacitance and compared with CNFs made *via* traditional electrospinning with only 8% PVA. The results show 10-fold enhancements in the specific capacitance of the CNF electrodes obtained through ChE over other CNFs electrodes made *via* conventional electrospinning. This enhancement originates primarily from the increased surface area achieved through the formation of the cavities in each nanofiber, a feature that can be further enhanced by increasing the number of KSM elements used. The improvement obtained through this synthesis technique, as well as the relatively mild conditions required for its operation, suggest the potential of ChE as an economical and scalable fabrication method for supercapacitors.

EXPERIMENTAL METHODS

Solution Preparation. The solutions used in the ChE experiments were prepared separately by dissolving the polymers (wt %) in deionized water. PVA (MW 89,000 g/mol) was purchased from Sigma Aldrich (Toluca, Mexico) and dissolved in deionized water (8, 10, and 12 wt %), both with and without the addition of (5 wt %) SDS (from Sigma Aldrich, Toluca, Mexico). SA, purchased from Sigma Aldrich, Toluca, Mexico, was mixed (at 2, 3, 4, and 5 wt %) in deionized water. PEO (MW 300,000 g/mol) was mixed (at 7 wt %) in deionized water.

ChE Setup and Parameters. ChE was performed by housing the prepared solutions, either PVA and SA or PEO and SA, in (5 mL) syringe barrels and fastening to a Chemyx's Fusion 200, 2-channel syringe pump, which controlled the flow of the solutions into the KSM element (Figure 1A). The KSM element was custom designed and fabricated with a stereolithographic 3D printer and fastened 10 cm above a custom-made rotating drum collector. The two solutions were fed into the KSM element *via* silicone tubing, and copper tape was attached to the tip of the KSM element to create an electrode. The electric field, responsible for the formation of the fibers, was created by a Spellman CZE1000R voltage supply connected between the copper spinneret and the collector. The appropriate applied voltage was determined by finding the minimum voltage at which the Taylor cone is formed, which has small variations due to differences in concentrations of the polymer solutions (10−12 kV for PEO/SA, 11−13 kV for PVA/SA with SDS, and 18−19 kV for PVA/SA without SDS). The rotating drum collector was grounded and set to spin at 5 rps to form an even rectangular textile mat.

SEM Characterization. SEM micrographs were collected with the EVO MA25 (Zeiss, Germany). For the polymer nanofibers, it was necessary first to sputter a thin coating (5 nm) of gold to eliminate distortions from charging effects. The same coating was not needed for the CNFs.

PiFM and AFM Characterization. PiFM (Molecular Vista, CA) is a nanomaterial characterization tool that enables nanoscale chemical imaging with down to 10 nm spatial resolution.[38] Here, a mechanical cantilever with a probe tip that interacts with the sample surface is exploited to measure local light−matter interactions. Using the noncontact mode, the cantilever is excited at its second mechanical eigenmode and stabilized nanometers from the sample surface. Then, the tip-sample junction is illuminated with focused light generated by a quantum cascade laser with modulation frequency $f_m = f_2 - f_1$. Because tip-sample intermolecular interactions are nonlinear with distance, f_m mixes with f_2, and beating signals at the sum (higher side band) and the difference (lower side band) frequencies are generated. In our setup, the lower side band is tuned such that it overlaps with the first mechanical eigenmode, where the PiFM signal is measured. The wavelength of light excitation is tuned to one of the vibrational resonances that correspond to polymer nanofiber mats. Upon absorbing light, the sample temperature increases, leading to thermal stress. Since the laser is modulated at f_m, thermal expansion is also modulated at f_m, leading to a measurable signal at f_1. In this manner, PiFM is used to probe nano-striations on micron-sized fibers. For the PEO/SA nanofibers, an excitation band for PEO at 1100 cm^{-1} was used for the greatest contrast between the PEO and SA layers. In contrast, for the PVA/SA nanofibers, the excitation band of PVA at 1449 cm^{-1} had the greatest contrast between the different material layers. AFM analysis of the pyrolyzed CNFs was carried with the same equipment, however, without the photoinduced component.

Rheological Characterization. The rotational and oscillatory rheological parameters were measured for each polymer solution of varying concentrations separately with the MCR-101 rheometer (Anton Paar, Austria) and cone measuring plate (CP50-1-SN28724, cone radius 50.5 mm, cone angle 1°, sample volume 1.5 mL) at 25.0 ± 0.1 °C (Figure 3C). The viscosity was calculated with $\eta = \tau/\gamma$, where τ is the shear stress and γ is the shear rate.[54] During the rotational test, the shear rate was ranged from 6 to 130 s^{-1}. The oscillatory shear measurements were performed with amplitude within the linear region (amplitude 10%) of the tested frequency range.

Carbon Nanofiber Synthesis. Synthesis of the carbon and SCNFs began with the formation of pure PVA nanofibers (8 wt % PVA and 5 wt % SDS in deionized water) *via* traditional electrospinning (single syringe needle, 10 kV applied voltage, and 10 cm working distance) and PVA/SA nanofibers (12 wt % PVA and 5 wt % SDS in deionized water and 4 wt % SA in deionized water) *via* ChE (13 kV applied voltage at 10 cm working distance), respectively. The resultant polymer nanofiber mats were then incubated for 24 h in a 20 mL flask with 200 mg of iodine at 100 °C to induce the crosslinking of the PVA chains into polyene (Figure 4B), which strengthened the carbon chains so that the fibers could survive the pyrolysis process.[47] The crosslinked PVA and PVA/SA mats were then placed in an OTF 1200X tube furnace under a 40 mL/min continuous nitrogen flow, which was then heated to 1000 °C at 2 °C/min and held at 1000 °C for 1 h before letting it cool to room temperature through natural convection.

Electrochemical Characterization. To characterize CNFs electrochemically, the nanofibers were first cut into 1 cm × 0.25 cm rectangular pieces and then connected to a copper wire with silver paint. Finally, PDMS was used to cover the painted area to prevent contamination of the electrochemical signal with corrosion as shown in Figure 4D. A traditional three-electrode setup with a platinum mesh counter-electrode, a Ag/AgCl reference electrode, and the wired CNF working electrode were all placed in a 50 mL Pyrex beaker. The electrochemical measurements were made in a 2 M $MgCl_2$ solution with a Versastat PalmSens 4 potentiostat. Capacitance measurements

https://doi.org/10.1021/acsami.1c05429
ACS Appl. Mater. Interfaces 2021, 13, 37455−37465

were calculated from eqs 2 and 3 from the data acquired from the cyclic voltammograms and GCD experiments. The capacitance was also measured by EIS through numerical fitting to an electric circuit model, as described by Bera*et al.*[50]

■ ASSOCIATED CONTENT

Supporting Information

The Supporting Information is available free of charge at https://pubs.acs.org/doi/10.1021/acsami.1c05429.

> Polymer combinations and fiber type obtained; PiFM characterization of the layered structure of chaotically electrospun nanofibers using a three-element KSM printhead of 7% PEO/4% SA; rheological characterization of the polymer solutions including complex viscosity, storage and loss modulus; topological analysis of SCNF and CNF surfaces using AFM and comparison of the enhancement in surface area in SCNFs with respect to CNFs; and equivalent circuit model to extract the double-layer capacitance (PDF)

■ AUTHOR INFORMATION

Corresponding Authors

Sunshine Holmberg − *Escuela de Ingeniería y Ciencias, Tecnologico de Monterrey, Monterrey, Nuevo Leon 64849, Mexico*; Email: sholmberg@tec.mx

Sergio Omar Martínez-Chapa − *Escuela de Ingeniería y Ciencias, Tecnologico de Monterrey, Monterrey, Nuevo Leon 64849, Mexico*; orcid.org/0000-0003-2689-1166; Email: smart@tec.mx

Grissel Trujillo-de Santiago − *Centro de Biotecnología-FEMSA and Departamento de Ingeniería Mecatrónica y Eléctrica, Escuela de Ingeniería y Ciencias, Tecnologico de Monterrey, Monterrey, Nuevo Leon 64849, Mexico*; orcid.org/0000-0001-9230-4607; Email: grissel@tec.mx

Authors

Norma Alicia Garza-Flores − *Centro de Biotecnología-FEMSA, Tecnologico de Monterrey, Monterrey, Nuevo Leon 64849, Mexico*; orcid.org/0000-0002-7880-2842

Mohammad Ali Almajhadi − *Department of Electrical Engineering and Computer Science, University of California, Irvine, Irvine, California 92697, United States*

Carolina Chávez-Madero − *Centro de Biotecnología-FEMSA, Tecnologico de Monterrey, Monterrey, Nuevo Leon 64849, Mexico*

Alejandro Lujambio-Angeles − *Escuela de Ingeniería y Ciencias, Tecnologico de Monterrey, Monterrey, Nuevo Leon 64849, Mexico*

Binny Jind − *Escuela de Ingeniería y Ciencias, Tecnologico de Monterrey, Monterrey, Nuevo Leon 64849, Mexico*; orcid.org/0000-0003-4143-7156

Claudia Bautista-Flores − *Escuela de Ingeniería y Ciencias, Tecnologico de Monterrey, Monterrey, Nuevo Leon 64849, Mexico*

Christian Mendoza-Buenrostro − *Centro de Biotecnología-FEMSA, Tecnologico de Monterrey, Monterrey, Nuevo Leon 64849, Mexico*; orcid.org/0000-0003-2509-0025

Esther Pérez-Carrillo − *Escuela de Ingeniería y Ciencias and Centro de Biotecnología-FEMSA, Tecnologico de Monterrey, Monterrey, Nuevo Leon 64849, Mexico*; orcid.org/0000-0003-2636-6281

Hemantha Kumar Wickramasinghe − *Department of Electrical Engineering and Computer Science, University of California, Irvine, Irvine, California 92697, United States*

Marc Madou − *Department of Mechanical and Aerospace Engineering, University of California, Irvine, Irvine, California 92697, United States*

Paul S. Weiss − *Department of Chemistry and Biochemistry, Department of Bioengineering, Department of Materials Science and Engineering, and California NanoSystems Institute (CNSI), University of California, Los Angeles, Los Angeles, California 90095, United States*; orcid.org/0000-0001-5527-6248

Mario Moisés Álvarez − *Centro de Biotecnología-FEMSA and Departmento de Bioingeniería, Escuela de Ingeniería y Ciencias, Tecnologico de Monterrey, Monterrey, Nuevo Leon 64849, Mexico*

Complete contact information is available at: https://pubs.acs.org/10.1021/acsami.1c05429

Author Contributions

S.H. and N.A.G.-F. contributed equally to this work. S.H., C.C.-M., M.M.Á., and G.T.-d.S. jointly conceived of the study. S.H. and N.A.G.-F. designed and performed the synthesis of chaotic nanofibers and analyzed the results. M.A.A., and B.J. performed the PiFM experiment and analysis. B.J. and C.B.-F. conducted the AFM-based characterizations. B.J. developed the algorithm to integrate the surface area density of ChE mats from AFM data. S.H., A.L.-A., B.J., and C.B.-F. synthesized the SCNFs and performed the electrochemical characterization and analysis. E.P.-C., S.H., and N.A.G.-F. performed and analyzed the rheology of the polymer solution supervised by E.P.-C. S.H. wrote the manuscript with contributions from N.A.G.-F., C.C.-M., B.J., M.M.Á., and G.T.-d.S. Additionally, C.C.-M. fabricated the custom KSM elements for the study. M.M.Á., G.T.-d.S., S.O.M.-C., H.K.W., and M.M. supervised the research team. All authors reviewed the manuscript.

Notes

The authors declare no competing financial interest.

■ ACKNOWLEDGMENTS

The authors would like to thank the (Consejo Nacional de Ciencia y Tecnología, México) CONACYT grant 249036, C0013-2014-02, ERANET-LAC for assisting in sponsoring this project. G.T.-d.S. acknowledges the funding received from CONACyT and L'Oréal-UNESCO-CONACyT-AMC (National Fellowship for Women in Science, Mexico). G.T.-d.S. and P.S.W. thank UC-MEXUS for the support of this work. S.O.M.-C., H.K.W., and M.M.A. gratefully acknowledge the funding provided by the Federico Baur Endowment Chair. G.T.-d.S. and M.M.Á. acknowledge the institutional funding received from Tecnológico de Monterrey (grant 002EICIS01). M.M.Á., G.T.-d.S., and S.O.M.-C. acknowledge the funding provided by CONACyT through grants SNI 26048, SNI 256730, and SNI 31803, respectively. We gratefully acknowledge the collaboration of Diego Alonso Quevedo-Moreno in the preparation of several of the schemes shown in the manuscript.

■ REFERENCES

(1) Bose, A.; Mal, P. Mechanochemistry of Supramolecules. *Beilstein J. Org. Chem.* **2019**, *15*, 881−900.

(2) Yan, Y.; Huang, J. Hierarchical Assemblies of Coordination Supramolecules. *Coord. Chem. Rev.* **2010**, *254*, 1072−1080.
(3) Brinke, G. T.; Ikkala, O. Smart Materials Based on Self-Assembled Hydrogen-Bonded Comb-Shaped Supramolecules. *Chem. Rec.* **2004**, *4*, 219−230.
(4) Mai, H. D.; Tran, N. M.; Yoo, H. Multilevel Coordination-Driven Assembly for Metallosupramolecules with Hierarchical Structures. *Coord. Chem. Rev.* **2019**, *387*, 180−198.
(5) Haider, A.; Haider, S.; Kang, I.-K. A Comprehensive Review Summarizing the Effect of Electrospinning Parameters and Potential Applications of Nanofibers in Biomedical and Biotechnology. *Arabian J. Chem.* **2018**, *11*, 1165−1188.
(6) Vigani, B.; Rossi, S.; Milanesi, G.; Bonferoni, M.; Sandri, G.; Bruni, G.; Ferrari, F. Electrospun Alginate Fibers: Mixing of Two Different Poly(Ethylene Oxide) Grades to Improve Fiber Functional Properties. *Nanomaterials* **2018**, *8*, 971.
(7) Kirillova, A.; Marschelke, C.; Synytska, A. Hybrid Janus Particles: Challenges and Opportunities for the Design of Active Functional Interfaces and Surfaces. *ACS Appl. Mater. Interfaces* **2019**, *11*, 9643−9671.
(8) Fan, X.; Yang, J.; Loh, X. J.; Li, Z. Polymeric Janus Nanoparticles: Recent Advances in Synthetic Strategies, Materials Properties, and Applications. *Macromol. Rapid Commun.* **2019**, *40*, 1800203.
(9) Poggi, E.; Gohy, J.-F. Janus Particles: From Synthesis to Application. *Colloid Polym. Sci.* **2017**, *295*, 2083−2108.
(10) Anker, J. N.; Kopelman, R. Magnetically Modulated Optical Nanoprobes. *Appl. Phys. Lett.* **2003**, *82*, 1102−1104.
(11) Behrend, C. J.; Anker, J. N.; McNaughton, B. H.; Kopelman, R. Microrheology with Modulated Optical Nanoprobes (MOONs). *J. Magn. Magn. Mater.* **2005**, *293*, 663−670.
(12) Han, Y. D.; Kim, H.-S.; Park, Y. M.; Chun, H. J.; Kim, J.-H.; Yoon, H. C. Retroreflective Janus Microparticle as a Nonspectroscopic Optical Immunosensing Probe. *ACS Appl. Mater. Interfaces* **2016**, *8*, 10767−10774.
(13) Wu, Z.; Li, L.; Liao, T.; Chen, X.; Jiang, W.; Luo, W.; Yang, J.; Sun, Z. Janus Nanoarchitectures: From Structural Design to Catalytic Applications. *Nano Today* **2018**, *22*, 62−82.
(14) Cao, W.; Huang, R.; Qi, W.; Su, R.; He, Z. Self-Assembly of Amphiphilic Janus Particles into Monolayer Capsules for Enhanced Enzyme Catalysis in Organic Media. *ACS Appl. Mater. Interfaces* **2015**, *7*, 465−473.
(15) Qin, W.; Peng, T.; Gao, Y.; Wang, F.; Hu, X.; Wang, K.; Shi, J.; Li, D.; Ren, J.; Fan, C. Catalysis-Driven Self-Thermophoresis of Janus Plasmonic Nanomotors. *Angew. Chem., Int. Ed.* **2017**, *56*, 515−518.
(16) Gao, W.; Wang, J. Synthetic Micro/Nanomotors in Drug Delivery. *Nanoscale* **2014**, *6*, 10486−10494.
(17) Shao, D.; Zhang, X.; Liu, W.; Zhang, F.; Zheng, X.; Qiao, P.; Li, J.; Dong, W.-f.; Chen, L. Janus Silver-Mesoporous Silica Nanocarriers for SERS Traceable and PH-Sensitive Drug Delivery in Cancer Therapy. *ACS Appl. Mater. Interfaces* **2016**, *8*, 4303−4308.
(18) Mou, F.; Chen, C.; Zhong, Q.; Yin, Y.; Ma, H.; Guan, J. Autonomous Motion and Temperature-Controlled Drug Delivery of Mg/Pt-Poly(N-Isopropylacrylamide) Janus Micromotors Driven by Simulated Body Fluid and Blood Plasma. *ACS Appl. Mater. Interfaces* **2014**, *6*, 9897−9903.
(19) Jurado-Sánchez, B.; Escarpa, A. Janus Micromotors for Electrochemical Sensing and Biosensing Applications: A Review. *Electroanalysis* **2017**, *29*, 14−23.
(20) Yi, Y.; Sanchez, L.; Gao, Y.; Yu, Y. Janus Particles for Biological Imaging and Sensing. *Analyst* **2016**, *141*, 3526−3539.
(21) Jurado-Sánchez, B.; Sattayasamitsathit, S.; Gao, W.; Santos, L.; Fedorak, Y.; Singh, V. V.; Orozco, J.; Galarnyk, M.; Wang, J. Self-Propelled Activated Carbon Janus Micromotors for Efficient Water Purification. *Small* **2015**, *11*, 499−506.
(22) Doshi, J.; Reneker, D. H. Electrospinning Process and Applications of Electrospun Fibers. *Conference Record of the 1993 IEEE Industry Applications Conference Twenty-Eighth IAS Annual Meeting*, 1993; vol. 3, pp 1698−1703.
(23) Zhang, B.; Kang, F.; Tarascon, J.-M.; Kim, J.-K. Recent Advances in Electrospun Carbon Nanofibers and Their Application in Electrochemical Energy Storage. *Prog. Mater. Sci.* **2016**, *76*, 319−380.
(24) Mao, X.; Hatton, T. A.; Rutledge, G. C. A Review of Electrospun Carbon Fibers as Electrode Materials for Energy Storage. https://www.ingentaconnect.com/content/ben/coc/2013/00000017/00000013/art00006 (accessed May 04, 2020).
(25) Ding, B.; Wang, M.; Wang, X.; Yu, J.; Sun, G. Electrospun Nanomaterials for Ultrasensitive Sensors. *Mater. Today* **2010**, *13*, 16−27.
(26) Angeles, M.; Cheng, H. L.; Velankar, S. S. Emulsion Electrospinning: Composite Fibers from Drop Breakup during Electrospinning. *Polym. Adv. Technol.* **2008**, *19*, 728−733.
(27) Zhang, C.; Zhang, H. Formation and Stability of Core−Shell Nanofibers by Electrospinning of Gel-Like Corn Oil-in-Water Emulsions Stabilized by Gelatin. *J. Agric. Food Chem.* **2018**, *66*, 11681−11690.
(28) Yarin, A. L. Coaxial Electrospinning and Emulsion Electrospinning of Core−Shell Fibers. *Polym. Adv. Technol.* **2011**, *22*, 310−317.
(29) Liu, X.; Yang, Y.; Yu, D.-G.; Zhu, M.-J.; Zhao, M.; Williams, G. R. Tunable Zero-Order Drug Delivery Systems Created by Modified Triaxial Electrospinning. *Chem. Eng. J.* **2019**, *356*, 886−894.
(30) Huang, W.; Wang, M.-J.; Liu, C.-L.; You, J.; Chen, S.-C.; Wang, Y.-Z.; Liu, Y. Phase Separation in Electrospun Nanofibers Controlled by Crystallization Induced Self-Assembly. *J. Mater. Chem. A* **2014**, *2*, 8416−8.
(31) Chávez-Madero, C.; de León-Derby, M. D.; Samandari, M.; Ceballos-González, C. F.; Bolívar-Monsalve, E. J.; Mendoza-Buenrostro, C.; Holmberg, S.; Garza-Flores, N. A.; Almajhadi, M. A.; González-Gamboa, I.; Yee-de León, J. F.; Martínez-Chapa, S. O.; Rodríguez, C. A.; Wickramasinghe, H. K.; Madou, M.; Dean, D.; Khademhosseini, A.; Zhang, Y. S.; Alvarez, M. M.; Trujillo-de Santiago, G. Using Chaotic Advection for Facile High-Throughput Fabrication of Ordered Multilayer Micro- and Nanostructures: Continuous Chaotic Printing. *Biofabrication* **2020**, *12*, 035023.
(32) Ma, M.; Krikorian, V.; Yu, J. H.; Thomas, E. L.; Rutledge, G. C. Electrospun Polymer Nanofibers with Internal Periodic Structure Obtained by Microphase Separation of Cylindrically Confined Block Copolymers. *Nano Lett.* **2006**, *6*, 2969−2972.
(33) Ma, M.; Hill, R. M.; Lowery, J. L.; Fridrikh, S. V.; Rutledge, G. C. Electrospun Poly(Styrene-Block-Dimethylsiloxane) Block Copolymer Fibers Exhibiting Superhydrophobicity. *Langmuir* **2005**, *21*, 5549−5554.
(34) García-Moreno, P. J.; Stephansen, K.; van der Kruijs, J.; Guadix, A.; Guadix, E. M.; Chronakis, I. S.; Jacobsen, C. Encapsulation of Fish Oil in Nanofibers by Emulsion Electrospinning: Physical Characterization and Oxidative Stability. *J. Food Eng.* **2016**, *183*, 39−49.
(35) Bolívar-Monsalve, E. J.; Ceballos-González, C. F.; Borrayo-Montaño, K. I.; Quevedo-Moreno, D. A.; Yee-de León, J. F.; Khademhosseini, A.; Weiss, P. S.; Alvarez, M. M.; Trujillo-de Santiago, G. Continuous Chaotic Bioprinting of Skeletal Muscle-like Constructs. *Bioprinting* **2021**, *21*, No. e00125.
(36) Ceballos-González, C. F.; Bolívar-Monsalve, E. J.; Quevedo-Moreno, D. A.; Lam-Aguilar, L. L.; Borrayo-Montaño, K. I.; Yee-de León, J. F.; Zhang, Y. S.; Alvarez, M. M.; Trujillo-de Santiago, G. High-Throughput and Continuous Chaotic Bioprinting of Spatially Controlled Bacterial Microcosms. *ACS Biomater. Sci. Eng.* **2021**, *7*, 2408−2419.
(37) Samandari, M.; Alipanah, F.; Majidzadeh-A, K.; Alvarez, M. M.; Trujillo-de Santiago, G.; Tamayol, A. Controlling Cellular Organization in Bioprinting through Designed 3D Microcompartmentalization. *Appl. Phys. Rev.* **2021**, *8*, 021404.
(38) Rajapaksa, I.; Uenal, K.; Wickramasinghe, H. K. Image Force Microscopy of Molecular Resonance: A Microscope Principle. *Appl. Phys. Lett.* **2010**, *97*, 073121.
(39) Rajaei, M.; Almajhadi, M. A.; Zeng, J.; Wickramasinghe, H. K. Near-Field Nanoprobing Using Si Tip-Au Nanoparticle Photoinduced

Force Microscopy with 120:1 Signal-to-Noise Ratio, Sub-6-Nm Resolution. *Opt. Express* **2018**, *26*, 26365−26376.
(40) Nowak, D.; Morrison, W.; Wickramasinghe, H. K.; Jahng, J.; Potma, E.; Wan, L.; Ruiz, R.; Albrecht, T. R.; Schmidt, K.; Frommer, J.; Sanders, D. P.; Park, S. Nanoscale Chemical Imaging by Photoinduced Force Microscopy. *Sci. Adv.* **2016**, *2*, No. e1501571.
(41) Arinstein, A. Confinement Mechanism of Electrospun Polymer Nanofiber Reinforcement. *J. Polym. Sci., Part B: Polym. Phys.* **2013**, *51*, 756−763.
(42) Baji, A.; Mai, Y.-W.; Wong, S.-C.; Abtahi, M.; Chen, P. Electrospinning of Polymer Nanofibers: Effects on Oriented Morphology, Structures and Tensile Properties. *Compos. Sci. Technol.* **2010**, *70*, 703−718.
(43) Lu, J.-W.; Zhu, Y.-L.; Guo, Z.-X.; Hu, P.; Yu, J. Electrospinning of Sodium Alginate with Poly(Ethylene Oxide). *Polymer* **2006**, *47*, 8026−8031.
(44) Safi, S.; Morshed, M.; Hosseini Ravandi, S. A.; Ghiaci, M. Study of Electrospinning of Sodium Alginate, Blended Solutions of Sodium Alginate/Poly(Vinyl Alcohol) and Sodium Alginate/Poly(Ethylene Oxide). *J. Appl. Polym. Sci.* **2007**, *104*, 3245−3255.
(45) Nista, S. V. G.; Bettini, J.; Mei, L. H. I. Coaxial Nanofibers of Chitosan−Alginate−PEO Polycomplex Obtained by Electrospinning. *Carbohydr. Polym.* **2015**, *127*, 222−228.
(46) Mirtič, J.; Balažic, H.; Zupančič, Š.; Kristl, J. Effect of Solution Composition Variables on Electrospun Alginate Nanofibers: Response Surface Analysis. *Polymers* **2019**, *11*, 692.
(47) Fatema, U. K.; Uddin, A. J.; Uemura, K.; Gotoh, Y. Fabrication of Carbon Fibers from Electrospun Poly(Vinyl Alcohol) Nanofibers. *Text. Res. J.* **2011**, *81*, 659−672.
(48) Śliwak, A.; Grzyb, B.; Ćwikła, J.; Gryglewicz, G. Influence of Wet Oxidation of Herringbone Carbon Nanofibers on the Pseudocapacitance Effect. *Carbon* **2013**, *64*, 324−333.
(49) Wasiński, K.; Walkowiak, M.; Lota, G. Humic Acids as Pseudocapacitive Electrolyte Additive for Electrochemical Double Layer Capacitors. *J. Power Sources* **2014**, *255*, 230−234.
(50) Bera, B.; Kar, T.; Chakraborty, A.; Neergat, M. Influence of Nitrogen-Doping in Carbon on Equivalent Distributed Resistance and Capacitance—Implications to Electrocatalysis of Oxygen Reduction Reaction. *J. Electroanal. Chem.* **2017**, *805*, 184−192.
(51) Kim, C.; Ngoc, B. T. N.; Yang, K. S.; Kojima, M.; Kim, Y. A.; Kim, Y. J.; Endo, M.; Yang, S. C. Self-Sustained Thin Webs Consisting of Porous Carbon Nanofibers for Supercapacitors via the Electrospinning of Polyacrylonitrile Solutions Containing Zinc Chloride. *Adv. Mater.* **2007**, *19*, 2341−2346.
(52) Tran, C.; Kalra, V. Fabrication of Porous Carbon Nanofibers with Adjustable Pore Sizes as Electrodes for Supercapacitors. *J. Power Sources* **2013**, *235*, 289−296.
(53) Azhar, A.; Yamauchi, Y.; Allah, A. E.; Alothman, Z. A.; Badjah, A. Y.; Naushad, M.; Habila, M.; Wabaidur, S.; Wang, J.; Zakaria, M. B. Nanoporous Iron Oxide/Carbon Composites through In-Situ Deposition of Prussian Blue Nanoparticles on Graphene Oxide Nanosheets and Subsequent Thermal Treatment for Supercapacitor Applications. *Nanomaterials* **2019**, *9*, 776.
(54) Gašperlin, M.; Tušar, L.; Tušar, M.; Šmid-Korbar, J.; Zupan, J.; Kristl, J. Viscosity Prediction of Lipophilic Semisolid Emulsion Systems by Neural Network Modelling. *Int. J. Pharm.* **2000**, *196*, 37−50.

https://doi.org/10.1021/acsami.1c05429
ACS Appl. Mater. Interfaces 2021, 13, 37455−37465